Characterization of non-thermal dielectric barrier discharges for plasma medicine : from plastic well plates to skin surfaces

Title: Characterization of non-thermal dielectric barrier discharges for plasma medicine: from plastic well plates to skin surfaces

Authors: Abraham Lin[1,2*], Mikhail Gromov[3], Anton Nikiforov[3], Evelien Smits[2+], Annemie Bogaerts[1+]

Affiliations:
[1] Plasma Lab for Sustainability and Medicine – Antwerp (PLASMANT), University of Antwerp, Universiteitsplein 1, 2610 Antwerp-Wilrijk, Belgium
[2] Center for Oncological Research, Integrated Personalized and Precision Oncology Network, University of Antwerp, Universiteitsplein 1, 2610 Antwerp-Wilrijk, Belgium
[3] Research Unit Plasma Technology (RUPT), Department of Applied Physics, Ghent University, Sint-Pietersnieuwstraat 41, 9000 Ghent, Belgium

[*] corresponding author email: abraham.lin@uantwerpen.be
[+] shared senior author

Abstract

In the past decade, the applications of dielectric barrier discharge (DBD) plasma technologies have been expanding, and one of the most exciting and rapidly growing applications is in biology and medicine. Most biomedical studies with DBD plasma systems are performed *in vitro*, which include cells grown on the surface of plastic well plates, or *in vivo*, which include animal research models (e.g. mice, pigs). Since many DBD systems use the biological target as the secondary electrode for direct plasma generation and treatment, they are sensitive to the surface properties of the target, and thus can be altered based on the *in vitro* or *in vivo* system used. This could consequently affect biological response from plasma treatment. Therefore, in this study, we investigated the DBD plasma behavior both *in vitro* (i.e. 96-well flat bottom plates, 96-well U-bottom plates, and 24-well flat bottom plates), and *in vivo* (i.e. mouse skin). Intensified charge coupled device (ICCD) imaging was performed and the plasma discharges were visually distinguishable between the different systems. The geometry of the wells did not affect DBD plasma generation for low application distances (≤ 2 mm), but differentially affected plasma uniformity on the bottom of the well at greater distances. Since DBD plasma treatment *in vitro* is rarely performed in dry wells for plasma medicine experiments, the effect of well wetness was also investigated. In all *in vitro* cases, the uniformity of the DBD plasma was affected when comparing wet versus dry wells, with the plasma in the wide-bottom wells appearing the most similar to plasma generated on mouse skin. Interestingly, based on quantification of ICCD images, the DBD plasma

intensity per surface area demonstrated an exponential one-phase decay with increasing application distance, regardless of the *in vitro* or *in vivo* system. This trend is similar to that of the energy per pulse of plasma, which is used to determine the total plasma treatment energy for biological systems. Optical emission spectroscopy performed on the plasma revealed similar trends in radical species generation between the plastic well plates and mouse skin. Therefore, taken together, DBD plasma intensity per surface area may be a valuable parameter to be used as a simple method for *in situ* monitoring during biological treatment and active plasma treatment control, which can be applied for *in vitro* and *in vivo* systems.

Introduction

Dielectric barrier discharge (DBD) systems are generated by applying voltage to one or two electrodes in order to ionize the gas in between them, where at least one electrode is covered by a dielectric material [1]. DBDs became a transformative technology in 1857, when Werner von Siemens reported on the design of a DBD for ozone generation. Since then, industrial applications of DBDs have expanded to include surface modifications [2], excimer-based lighting [3], and even pollution control [4]. The significance and influence of DBD technologies leading to the early 2000s was summarized by the late Professor Ulrich Kogelschatz, one of the most prominent scientists in the field [5]. His review, published in 2003, has over 2300 citations in Web of Science and continues to be referenced each year [5]. Since then, the applications of DBDs have continued to expand, and one of the most exciting and rapidly growing applications is in biology and medicine [6].

DBD plasma devices are able to generate electrically and thermally safe plasmas, and they have been used for a variety of medical and biomedical applications in a field now coined as ‘plasma medicine’. Many biomedical DBD devices use the biological target as the second electrode and generate plasma directly onto the cells or tissue to be treated. They are characterized by generating non-thermal plasma near room temperature ($\leq 40^{o}C$) and at atmospheric pressure and thus, do not rely on thermal properties to induce therapeutic effects [7]. Instead, several studies have demonstrated that the reactive oxygen and nitrogen species (RONS) generated by DBD plasma are most responsible for eliciting biological responses [8-11]. Biological applications of DBD plasma currently under investigation include: blood

coagulation [12-14], wound healing [14-16], neuroregeneration [17-19], inactivation of microorganisms [20-22], and cancer treatment [23-25]. The wide range of biomedical applications associated with DBD plasma treatment has been linked to the 'intensity' of the treatment and the RONS responsible for eliciting an effect [6]. For example, several studies have demonstrated that short-lived RONS, particularly the hydroxyl radical (●OH), atomic oxygen and ozone (●O/O_3), and nitric oxide (●NO) are most responsible for inducing immunogenic cell death in melanoma cancer cells [8, 9], while ●NO and other NO derivatives have also been proposed to enhance blood circulation and potential wound healing [16]. Furthermore, low 'intensities' of DBD plasma treatment have been shown to promote cell proliferation, while higher 'intensities' become detrimental and induce cell death. As such, defining 'plasma treatment dose' for different biological applications has become critical for successful translation of DBD plasma devices (among other non-thermal plasma devices) from the research lab into the clinic [26]. Our lab has begun to delineate the contribution of different DBD plasma treatment parameters (e.g. pulse frequency, treatment time, application distance) on downstream cancer cell death and we reported that the plasma treatment energy delivered to cancer cells encompasses the effects of several application parameters, *in vitro* [27].

Still, another gap in understanding is on the differences between how DBD plasma interacts with biological samples *in vitro* versus *in vivo*. Since DBD systems use the biological target as the secondary electrode for direct plasma generation and treatment, they are sensitive to the surface properties of the target [28, 29]. In most *in vitro* settings, this surface includes cells grown on plastic culture well plates, while *in vivo*, this surface constitutes the skin or tissue of patients or animal research models (e.g. mice). Already several studies have characterized DBD plasma using different experimental methods (e.g. fast imaging, power measurements) [28-30] and many groups have also worked to computationally model the interaction of DBD plasma on different biological surfaces and molecules [31, 32]. Most interestingly, Stancampiano, et al. has previously proposed implementing a basic electrical circuit to compensate for the electrical differences between *in vitro* models, *in vivo* mouse models, and even in humans [33]. While these studies were performed with a plasma jet and not a DBD plasma system, the authors highlighted the importance of taking into account the electrical characteristics of the treatment

target, and attempted to ease the translation of *in vitro* plasma experiments to the clinic by accounting for these electrical differences. Still, the compensation circuit alone was not sufficient to reconcile the *in vitro* treatment setting into a that of a human body.

In this study, we focused on investigating the DBD plasma behavior both *in vitro,* interacting with cell culture plates of several different geometries, and *in vivo,* interacting with mouse skin. Using fast imaging with an intensified charge coupled device (ICCD) camera, we observed plasma generation on the different surfaces and over a range of application distances. The energy per pulse of DBD plasma was also calculated from the measured voltage and current waveforms. Optical emission spectroscopy (OES) was performed to measure the reduced electric field, gas and vibrational temperatures, and to obtain insights into radical species generation in the DBD plasma. The DBD plasma discharge interacting with the well plates appeared visibly different based on the surface geometry, with discharges on larger diameter well plates appearing more similar to that of plasma interacting with *in vivo* mouse skin. From the images, we calculated the plasma interaction area on the surface of the target and the plasma intensity per surface area. The latter demonstrates an exponential one-phase decay with increasing application (gap) distance, and this trend closely follows the behavior of DBD plasma energy per pulse. These data highlight the potential use of DBD plasma intensity per surface area for *in situ* monitoring during biological treatment. Based on the OES data, only the vibrational temperature of N_2 excited states in the DBD plasma was significantly different between discharges on cell culture plates and mouse skin, which can be prescribed to the presence of different quencher sets, particularly to O_3 accumulation in the culture plates. Furthermore, generation of ●OH, atomic ●O, and ●NO was measured in all cases and these species demonstrated a similar trend regardless of the discharge surface. Taken together, we have compared the DBD plasma behavior interacting with various surfaces that are relevant for plasma medicine studies, which could affect downstream biological responses. This should be considered to better bridge the gaps between *in vitro*, *in vivo*, and future clinical studies. Furthermore, monitoring DBD plasma intensity per surface area may be a simple and valuable method to determine 'plasma treatment dose' *in situ* during biological treatment both in the lab and potentially in the clinic, though further studies and validation are still required.

Experimental Methods

Dielectric barrier discharge plasma system and treatment

A microsecond-pulsed DBD system was used to generate non-thermal plasma (Figure 1). This DBD plasma system was used in our previous investigation into plasma for cancer treatment applications [7, 23, 27, 34, 35]. A high-voltage power supply (Megaimpulse Ltd., Russia) generated an output voltage of 30 kV with a pulse width of 2 μs and a rise time fixed within 1 – 1.5 μs. The pulse frequency was adjusted and used in the range from 100 – 1000 Hz. The DBD applicator was also used in our previous work and comprised of a quartz-covered, copper-core electrode (DBD electrode). The DBD electrode was composed of a copper core (3 mm tip diameter) covered with a clear fused quartz tube having a 5 mm outer diameter and 25.4 mm length with one full radius, closed-rounded end. The tip of the DBD electrode (5 mm diameter) was positioned above the treatment target with a z-positioner and plasma was generated over a range of application distances (1 – 10 mm). A function generator (TG25T2A, TTI, Inc.) was used to externally trigger the high voltage power supply, and plasma was generated on the surface of different cell culture plates (Table 1), as well as on the surface of mouse skin. For all well plates, an outer frame is normally present which prevents the individual wells from touching the surface it is placed on. During DBD plasma treatment, this could cause plasma to be generated not only inside the well, but also between the well and the ground. Therefore, a conductive plate was cut to fit within the well plate frame and used to ensure that the bottom of the well was in direct contact with the grounded plate (contact plate, Figure 1 insert). This insert has also been used in all our previous *in vitro* plasma medicine experiments with the DBD plasma system, and the effect of this gap between the bottom of the well and the grounded plate should always be carefully considered when performing experiments with biological material.

For mouse experiments, female, C57BL/6J, 8-week-old mice were purchased from Charles River and housed in a pathogen-free room at the Animal Center of the University of Antwerp until sacrifice, as approved by the University of Antwerp Animal Research Ethical Committee (ECD-dossier 2017-53). The mouse was placed on a grounded, conductive plate for DBD plasma discharge, as described and

depicted in Figure 2 of our previous work [7]. The DBD electrode was then lowered onto the mouse skin with the Z-positioner, which was used to define the gap distances during treatment.

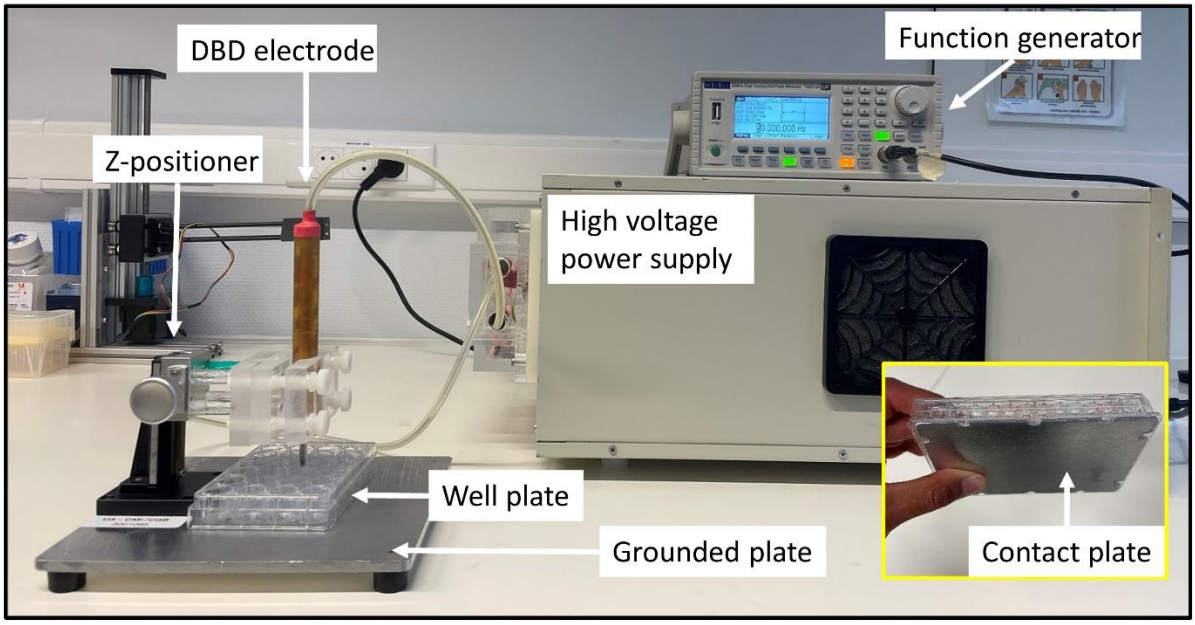

Figure 1. The microsecond-pulsed DBD plasma system used in this study. This system was also used in our previous plasma medicine work [27, 35, 36]. A contact plate (yellow insert) was used to fit within the well plate frame to ensure that the bottom of the well was in direct contact with the grounded plate.

Table 1. Cell culture plates used, along with abbreviations and well diameters and thicknesses

Well plate	Abbreviation	Well diameter	Well thickness
96-well flat bottom (Greiner Bio-One, 655180)	flat-bottom	6.58 mm	1.00 mm
96-well U-bottom (Corning, 7007)	U-bottom	6.35 mm	1.14 mm
24-well flat bottom (Greiner Bio-One, 662160)	wide-bottom (for ICCD imaging)	15.70 mm	1.20 mm
6-well flat bottom (Greiner Bio-One, 657160)	wide-bottom (for power and OES measurements)	35.58 mm	1.20 mm

ICCD camera imaging

An ICCD camera is a powerful tool for plasma visualization, especially for high frequency, short pulse plasmas with low emissivity signal, such as atmospheric pressure DBDs. This visualization technique allows for the monitoring of basic plasma parameters, which are crucial for understanding induced

biomedical effects. Specifically, the obtained images can be used for phenomenological characterization of a plasma, providing basic, but important plasma parameters such as:

- the plasma volume, which is proportional to the number of the generated chemically reactive products: at fixed ambient conditions (pressure, gas composition), a larger plasma volume → more atoms/molecules are excited → more chemically active species formed;
- plasma-surface interaction area, which represents a thin layer (typically a few hundred micrometers at atmospheric pressure conditions) where short-lived species exist and react with the substrate under investigation.

Finally, considering the main excitation and de-excitation pathways of the species under investigation (collisional-radiative modeling), the total emission signal can be attributed to the plasma ground state density of the RONS.

In this work, plasma imaging was used to illustrate the difference between the plasmas generated above plastic well plates, commonly used for treating *in vitro* biological cultures, and plasma generated above skin tissue; thus highlighting possible deviations in the observed results moving from *in vitro* to *in vivo* tests. The measurements were performed using a Hamamatsu ICCD camera with camera gate width of 10 μs and integrated over 25 camera shots. Considering the geometry of the systems under investigation, the analysis was performed using the regions of interest starting from the edge of the DBD electrode, as shown in Figure 2.

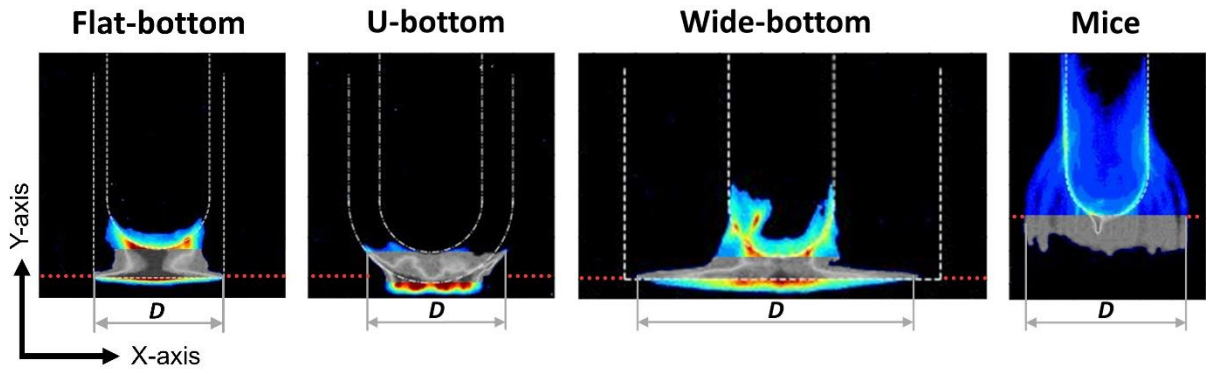

Figure 2. Schematic showing the investigated systems and regions of interest (ROI), used for calculating the plasma-treated surface areas, plasma volumes, and plasma intensities. Reference images were used to outline the edges of the DBD electrode and walls of the well plate (white dashed line) and the bottom of the well (y_0; red dotted line). Abbreviations: U-bottom (96-well U-bottom plate), flat-bottom (96-well flat bottom plate), wide-bottom (24-well flat bottom plate).

The total plasma intensity discussed in this work was calculated as:

$$I_0 = \frac{\sum_{x_0}^{x} \sum_{y_0}^{y} I}{G \cdot \Omega}$$

where I is the total emission signal in the region of interest (ROI, Figure 2), G is the efficiency of the optical system, which includes the signal detection efficiency of the camera and the lens, signal amplification, the camera integration time, and transparency of the WPs. The latter was measured using a UV-VIS spectrophotometer (UV mini-1240, Shimadzu, Japan) and was considered for calibrating the images as well as the rest of the mentioned factors. At the same time, Ω, the detection system's solid angle, can be neglected if the camera position is kept constant with respect to the plasma, as had been done during the measurements.

The plasma-treated surface area was estimated based on the assumption that the plasmas had axial symmetry and was calculated according to the equation below:

$$Plasma - treated\ surface\ area = \pi \left(\frac{D}{2}\right)^2$$

where D is the diameter of the plasma-treated surface area in mm, as illustrated in Figure 2.

The plasma volume was determined as the sum of the volumes in every vertical line of pixels in the image from y_0 to y in the region of interest and was calculated as follows:

$$V = \sum_{y0}^{y} V_{y_n} = \sum_{y0}^{y} \pi \cdot R_{y_n}^2 \cdot h$$

Here, R is the plasma radius in the vertical line n, and h is the height of one vertical line, both in mm.

Optical emission spectroscopy

At atmospheric pressure, high-frequency collisions between species lead to a fast rotational/translational equilibrium in the system [37, 38]. Therefore, the gas (translational) temperature is assumed to be equal to the rotational temperature. Thus, the gas (T_{gas}) and vibrational (T_{vib}) temperatures of the DBD were obtained assuming a Boltzmann distribution of the N_2 second positive system (SPS) simulating it in MassiveOES software [39, 40]. T_{gas} was obtained using the N_2 transition v'-v" = 0-0, of which the head is around 337 nm, while four vibrational peaks 0-2, 1-3, 2-4, and 3-5,

heading between 380.4 and 375 nm, were used to estimate the vibrational temperature of the N_2 electronically excited state. It must be mentioned that T_{gas} determination requires detecting a well resolved rotational structure. Therefore, a high resolution (0.05 nm) spectrometer Avantes-3648 was used to record the N_2(C-B, $\Delta v = 0$) transition.

The reduced electric field (*E/N*, i.e., the ratio of the applied electric field *E* and the neutral gas density *N*) is the main plasma parameter determining the electron energy and the dynamics of electron impact reactions. It defines the electron generation mechanisms, and consequently, the electron-initiated chemical kinetics. In DBD plasmas where electron impact electronic excitation is dominant, taking the ratio of two plasma-induced optical emission signals from two different radiative states with a significant difference in excitation energies is a well-established approach to estimate *E/N*. In this work, we used the spectral band intensities originating from the first negative and second positive spectral systems of N_2^+ and N_2, respectively. In this case, the intensity ratio of the two emission lines can be recalculated to the *E/N* value via a set of equations described elsewhere [41, 42].

Finally, optical emission spectra provide the intensities related to the density of excited species. However, the measured intensities can be correlated to ground state densities assuming that excitation mainly occurs through electron impact from the ground state (the so-called corona approximation). The estimation was performed considering that there was no collisional excitation, the excitation probability was determined employing a Maxwell electron energy distribution, de-excitation processes did not go through V-V and V-T energy transfer and charge exchange. In this work, we applied this approach to compare the behavior of the radicals, namely ●OH, ●O atoms, and ●NO in the investigated systems. A detailed description of the method can be found elsewhere [43], and the constants used for the calculation are presented in APPENDIX I. In this work, both *E/N* and the relative density of the species were estimated by using optical emission spectra in the wide spectral range from 250 to 900 nm, collected using an Ocean Optics S2000 spectrometer with a resolution of 1.7 nm (FWHM).

Power measurments

The voltage and current were measured in a 6-well plate with bottom thickness of 1.27 mm or on the surface of the mouse skin, as described in our previous work (Figure 3A) [27]. The voltage was

measured with a 1000× high-voltage probe (P6015A, Tektronix), while the current was measured with a current monitor (4100, Pearson Electronics, Inc.), and both waveforms were recorded on an oscilloscope (DSOX1102G, Keysight) (Figure 3B). A 50-ns sampling rate was used and 64 pulses were averaged. The energy of a single plasma discharge ($\varepsilon_{\text{discharge}}$) was calculated from the instantaneous voltage ($V_k(t)$) and instantaneous current ($I_k(t)$):

$$\varepsilon_{discharge} = \sum_{k=1}^{n} |V_k(t) \times I_k(t)| \times \Delta t,$$

Here, n is the number of recorded samples and the sampling time (Δt) was 50 ns. The energy per pulse from the displacement current was also measured by operating the high voltage power supply when the DBD electrode was 30 mm above the treatment surface. This value ($\varepsilon_{\text{displacement}}$) was subtracted from the $\varepsilon_{\text{discharge}}$ in order to calculate the plasma treatment energy per pulse ($\varepsilon_{\text{pulse}}$):

$$\varepsilon_{pulse} = \varepsilon_{discharge} - \varepsilon_{displacement}$$

This was measured for DBD plasma treatment on the different cell culture wells and on the mouse surface, over a range of application distances (1 – 17 mm).

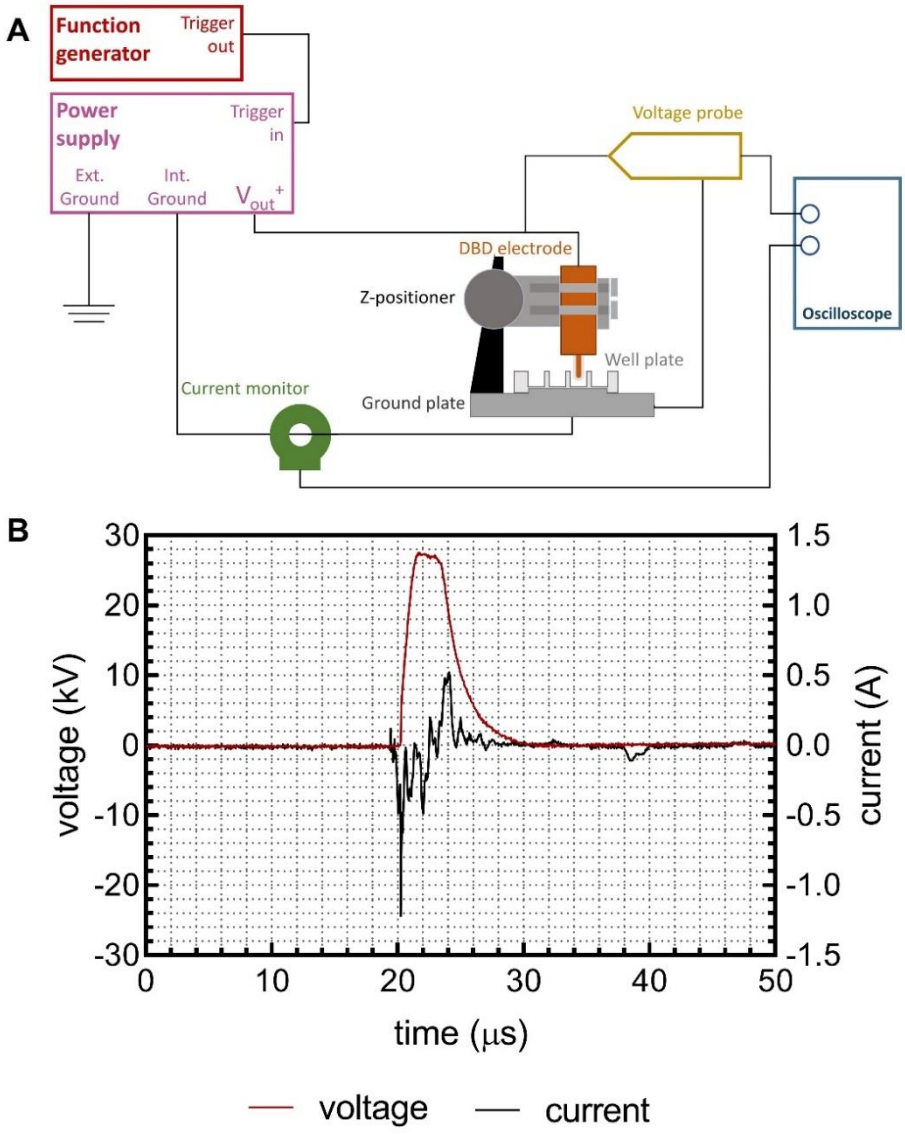

Figure 3. Experimental setup for power measurements. A) Schematic of the experimental setup, where the voltage and current of the DBD plasma discharge were measured using a voltage probe and current monitor, respectively, and recorded on an oscilloscope. B) Sample voltage and current waveform.

Results and Discussion

Geometry of cell culture well plates affects DBD plasma discharge

Most *in vitro* biological experiments with DBD plasma devices are performed in cell culture plates, which may have different geometries, depending on the biological model. For example, cells are grown on well plates with different well diameters, depending on the size of the DBD electrode [29, 44-46]. In most situations, these decisions are made based on a balance between the ability to lower the DBD electrode into the bottom of the well and to generate plasma over a majority of the cell surface for uniform treatment. Moreover, as 3D *in vitro* cell models are becoming more adopted for research [47,

48], the use of U-bottom plates for plasma treatment will become more prominent compared to the traditional flat-bottomed well plates [24, 49-51]. The geometry of the cell culture plates can affect cell morphology, organization, growth, density, and subsequently biological results from DBD plasma treatment, but here we investigated how different well plate geometries can also affect the DBD plasma discharge itself.

Using our microsecond-pulsed DBD plasma system operated at 30 kV and 700 Hz pulse frequency with a DBD electrode composed of a copper core (3 mm tip diameter) covered with a clear fused quartz tube (5 mm outer diameter, 25.4 mm long with long with one rounded, closed end). Plasma was generated in cell culture well plates with different geometries: 96-well flat bottom plate, 96-well U-bottom plate, and 24-well flat bottom plate (Table 1). An ICCD camera was used to image the plasma generated over a range of distances from 1 – 7 mm (Figure 4). Reference images were taken for each system (top) to identify the position of the DBD electrode in relation to the well plate (white dotted line) and overlaid on top of the ICCD image (bottom). At 1 and 2 mm application distances, plasma nearly covered the entire bottom surface of the well plate, regardless of geometry. As the application distance increased, the plasma channel visibly narrowed, and the contact surface of the plasma on the plastic was also minimized. For the 96-well flat bottom plate, plasma was still distributed across the bottom of the plate up to 5 mm application distance (Figure 4A), while both the U-bottom plate and the 24-well flat bottom plate had narrowing of the plasma channel and lower surface distribution at 3 mm and above (Figure 4B,C). DBD plasma was still observed at 7 mm application for both the 96-well flat bottom and U-bottom plate, but discharge was not observed anymore at 5 mm for the 24-well flat bottom plate (Figure 4C). Plasma pulse frequency (200 – 1000 Hz) did not visibly affect plasma generation for any of the three plate geometries (APPENDIX II).

Taken together, it is clear that the geometry of the well plates – both diameter of the wells and shape of the bottom – affects DBD plasma generation, especially over different application distances. This could affect downstream biological responses, as the density of the cells in the well (and thus cells treated with plasma) is often linked to the well size. While cells in a 96-well flat bottom plate treatment could be uniformly treated with plasma across a range of application distances, cells at the edges of the 24-

well plate would not directly interact with DBD plasma at application distances above 2 mm. Furthermore, the positioning of biological targets, such as spheroids, should be carefully considered above 3 mm treatment as the plasma surface is greatly reduced.

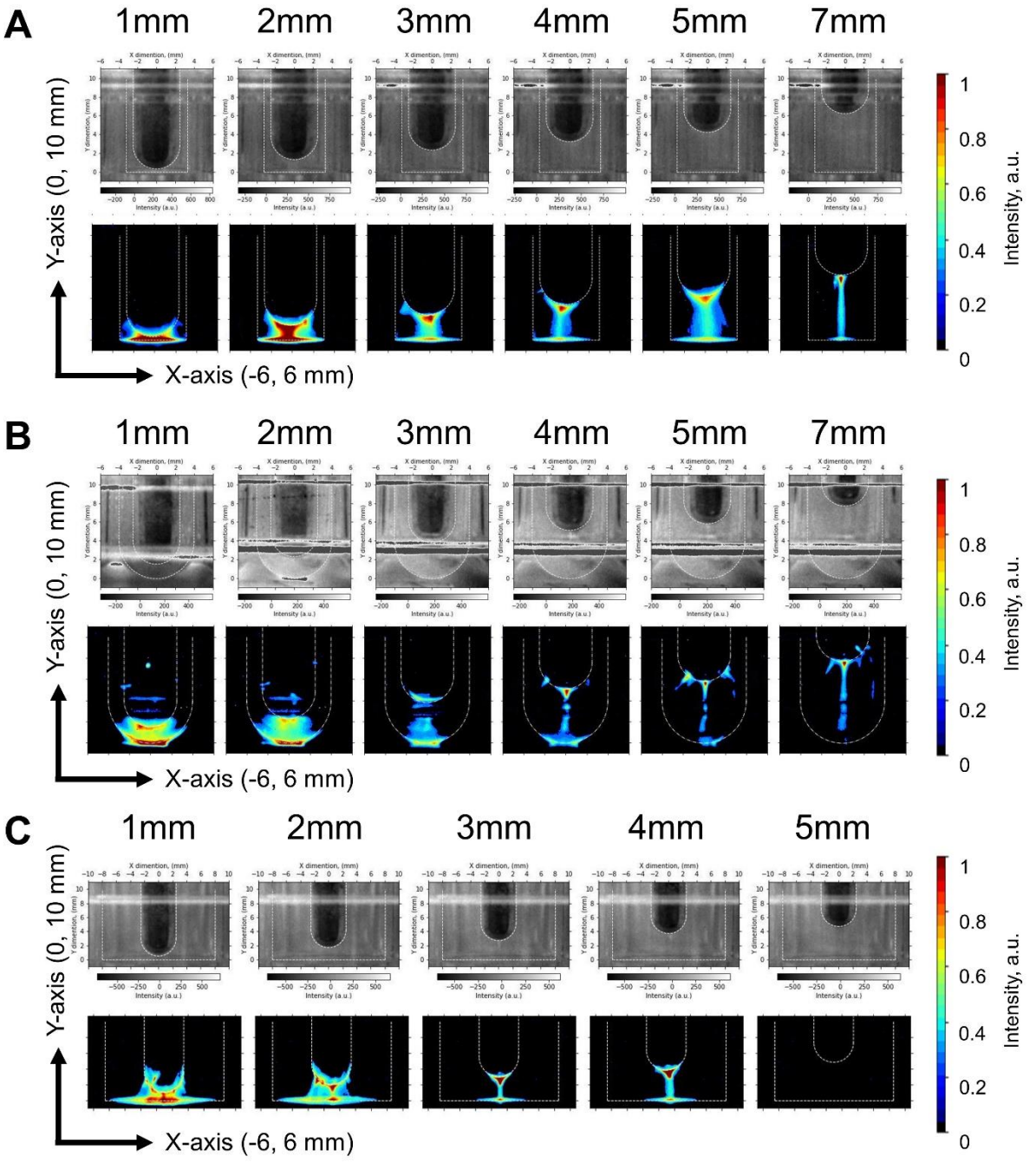

Figure 4. Effect of well plate geometry on DBD plasma. A DBD plasma was generated on a dry A) 96-well flat bottom plate, B) 96-well U-bottom plate, and C) 24-well flat bottom plate (wide-bottom plate) over several different application distances, as indicated above each panel. Reference images (top) were used to outline the edges of the DBD electrode and the walls and bottom surface of the well plate (white dotted line), and fast-imaging was used to capture plasma impingement on the plastic plate surface (bottom).

Wetness of cell culture well plates affects DBD plasma discharge

While the above experiments were performed on dry cell culture plates, in most *in vitro* biological experiments with DBD plasma, the biological samples are cultured in a liquid (e.g. culture medium, phosphate buffered saline), which is only removed right before DBD plasma treatment. Since most biological samples cannot be dried and residual liquid will always remain in the well, DBD plasma treatment is applied to wet cell culture plates. Therefore, we investigated the differences between DBD plasmas discharged on wet and dry cell culture plates for the different geometries.

Phosphate buffered saline was added into each well and removed right before treatment, as performed in our previous experiments [9]. DBD plasma was then again generated in the wells over a range of application distances, and ICCD imaging was used to capture the plasma. Once again, plasma pulse frequency (200 – 1000 Hz) did not visibly affect plasma generation for any of the three plate geometries (APPENDIX III), and representative images of the 700 Hz pulse treatment are shown for all well plates in Figure 5. Interestingly, for all well plates, the DBD plasma was visibly altered with wet wells compared to the dry wells (Figure 4). The DBD plasma channel and distribution across the bottom surface was distinctly reduced for both the 96-well flat bottom (Figure 5A) and the 24-well flat bottom plate (Figure 5C). For the U-bottom plate, plasma appeared to be discharging on the walls of the wells, as observed by the spotted distribution of the plasma along the well (Figure 5B).

Taken together, it is clear that the wet bottom of the cell culture plates affects the DBD plasma, which can affect how biological samples are treated. In particular, the plasma-treated area appears reduced when the wells are wet, which could affect the uniformity of treatment. For the U-bottom plate specifically, there appears to be more DBD discharge to the walls of the wells at higher distances, and this should be considered when performing DBD plasma experiments with 3D cell models, such as spheroids.

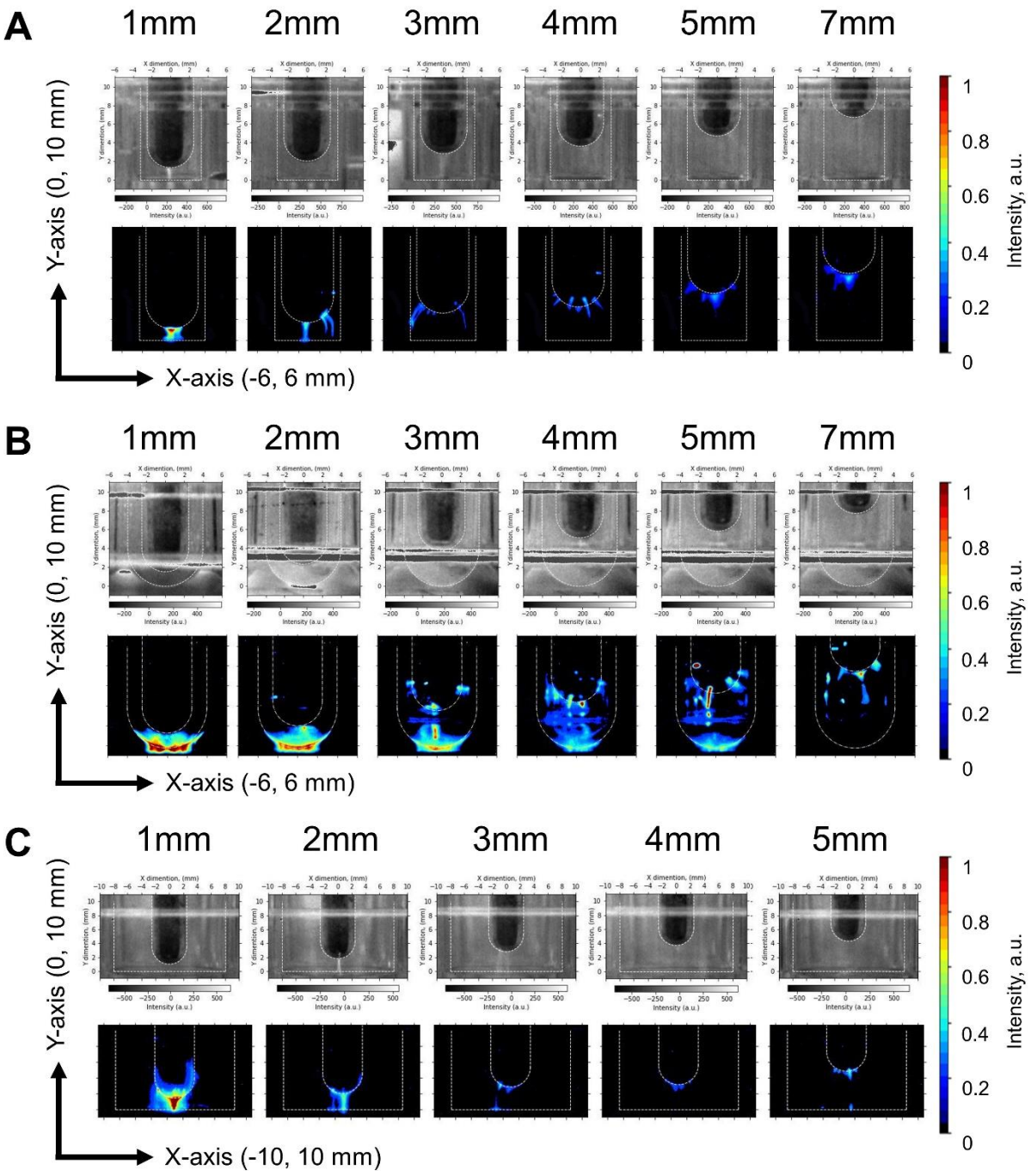

Figure 5. Effect of wet culture plates on DBD plasma for different plate geometries. Phosphate buffered saline (PBS) was added to each well and removed before DBD plasma generation, as commonly done for direct DBD plasma treatment of cell cultures. DBD plasma was then generated on wet A) 96-well flat-bottom plates, B) 96-well U-bottom plates, and C) 24-well flat bottom plates (wide-bottom plate) over several different application distances, as indicated above each panel. Reference images (top) were used to outline the edges of the DBD electrode and the walls and bottom surface of the well plate (white dotted line), and fast-imaging was used to capture plasma impingement on the plastic plate surface (bottom).

DBD plasma discharge on mouse skin

Following *in vitro* experiments, *in vivo* experiments are normally performed for more in-depth investigations in plasma medicine. Our lab, among others, has performed DBD plasma treatment experiments on tumor-bearing mice models [7, 11], and other labs across the world have also used *in vivo* mouse models for other plasma applications [52-55]. Therefore, we studied how DBD plasma treatment would distribute on the surface of mouse skin. The mouse was placed on a grounded, conductive plate for DBD plasma discharge, as described and further depicted in Figure 2 of our previous work [7].

The DBD plasma, operated at 700 Hz above the mouse skin, behaved similarly between application distances of 1 and 2 mm (Figure 6). At 3 and 4 mm, the plasma channel was visibly narrowed and the impinging surface on the skin was significantly reduced. Much like the 24-well flat bottom plate, the DBD plasma was not generated at an application distance of 5 mm above the skin surface of the mouse (Figure 6). Here, two DBD plasma treatment pulse frequencies were used (700 – 1000 Hz) and no major differences were observed (APPENDIX IV). Taken together, these data indicate that direct DBD treatment *in vivo*, and potentially in the clinic, should be applied between 1 – 2 mm for more uniform plasma treatment and greater deviations in application distance could affect the efficacy of treatment.

Based on the ICCD images taken from all *in vitro* and *in vivo* settings, it is clear that there are major differences between the various culture plate systems and mouse skin. With smaller well diameters, there appears to be a greater likelihood of discharging to the sides of the well at large gap distances, especially with a wet plate (Figure 5). This is particularly crucial to account for, as most biological experiments with DBD plasma are not performed in dry conditions. Therefore, it is highly suggested that DBD plasma treatments be performed as close to the treatment surface as possible. Furthermore, with a smaller well diameter, the intensity of the plasma on the bottom surface is much greater and the plasma-treated surface area is not as affected by application distance. It is important to consider here that this scenario may not be as closely representative of the *in vivo* and future clinical settings. The wide-bottom plate may be considered as more representative than the smaller well plates, as observed

when comparing the DBD plasma images on the wide-bottom plate (Figure 4C) to that of the mouse skin (Figure 6).

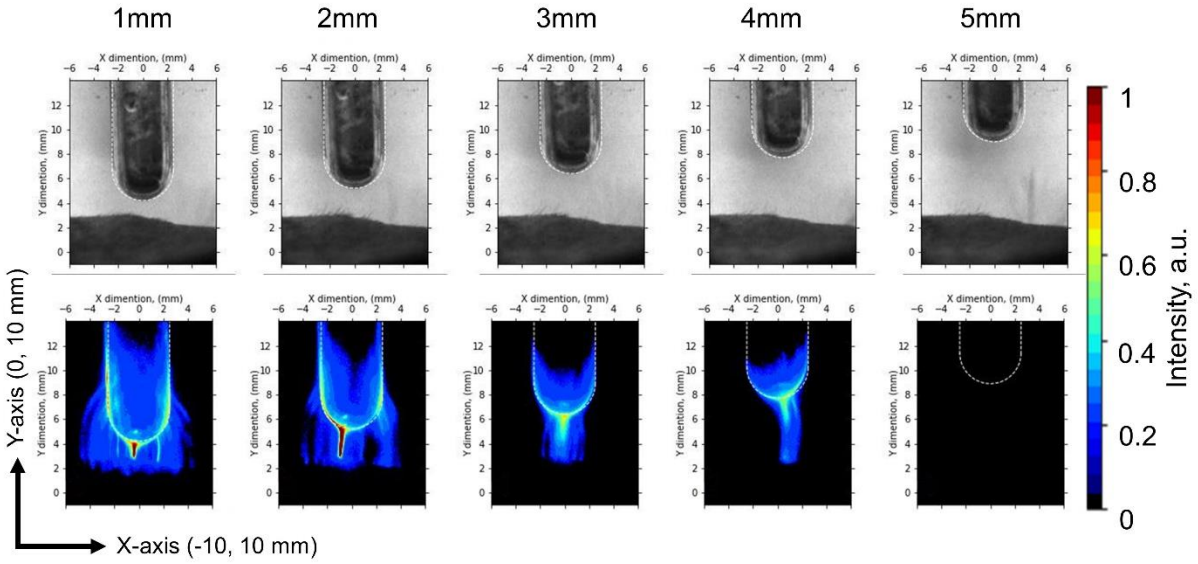

Figure 6. DBD plasma discharge on mouse skin. DBD plasma was generated directly on the skin of a mouse at varying application distances, as indicated above each panel. Reference images (top) were used to outline the edges of the DBD electrode above the mouse (white dotted line) and fast-imaging was used to capture plasma impingement on the surface of the mouse (bottom).

Quantification and comparison of DBD plasma discharge on plastic cell culture plates and mouse skin

In order to compare DBD plasma treatment in *in vitro* well plates and on *in vivo* mouse skin, we analyzed the trends of the total plasma intensities and cross-sectional areas of the plasma from the images. For nearly all treatment settings, the DBD plasma intensity decreased with increasing application distance (Figure 7A). However, the cross-sectional area of the plasma generally increased with increasing distance, to a certain point, before decreasing (Figure 7B). This is likely due to the ability of the plasma to fill the gap between the electrode and the target, up to a certain point before the plasma becomes too weak to sustain itself. From these measurements, we calculated the surface area of the DBD plasma on the target, as well as the volume of the plasma between the electrode and the target (APPENDIX V), as described above in Experimental Design (Figure 2). These data were used to calculate the DBD plasma intensity per surface area, using a fixed ROI with a 1 mm height, and the DBD plasma intensity per volume, using a fixed ROI between the two electrodes, respectively (Figure

2). We observed a similar trend for the DBD plasma intensity per surface area as a function of application distance, for all treatment conditions on the cell culture well plates and on the mouse skin (Figure 7C). In fact, for all conditions, an exponential one-phase decay behavior was observed with high correlation ($R^2 = 0.94 \pm 0.05$). The behavior of DBD plasma intensity per surface area as a function of application distance makes intuitive sense, and could have implications for biological treatments, as cells grown on that surface would experience the strongest effect from the interaction with plasma-generated species. This trend was not applicable for DBD plasma intensity per volume (APPENDIX V), as the volume of plasma dramatically decreased from 2 to 3 mm in the mouse treatments, while these changes were not measured for the well plates. Therefore, it appears that DBD plasma intensity per surface area as a function of application distance demonstrates a representative trend for all *in vitro* and *in vivo* systems studied here.

To investigate this further, the voltage and current of a single DBD plasma pulse were measured on a wide, flat bottom plate (6-well plate as performed in our previous publication [27]) and the mouse skin, as described in our previous publication [7]. At a 1 mm application distance, the energy per pulse was 2.93 ± 1.70 mJ/pulse and 1.76 ± 1.15 mJ/pulse for DBD plasma application on the dry and wet cell culture well plate, respectively (Figure 7D). As application distance increased, the energy per pulse decreased, as expected. This trend closely follows what we observed in our previously published work using the same DBD plasma system on mice, where at a 1 mm application distance, the energy per pulse was 1.08 ± 0.57 mJ/pulse, and decreased with increasing distance from the mouse skin [7] (Figure 7D). Furthermore, we have previously reported that DBD plasma-induced cancer cell death decreased with increasing application distance and decreasing plasma-treatment energy [27].

Taken together, it appears that for all treatment scenarios (i.e. dry and wet cell culture plates and mouse skin), the behavior of DBD plasma intensity per surface area (Figure 7C) is in-line with the energy per pulse of the discharge (Figure 7D), as well as published biological responses [7, 27]. These data are insightful and highlight the potential use of DBD plasma intensity per surface area for *in situ* monitoring during biological treatment.

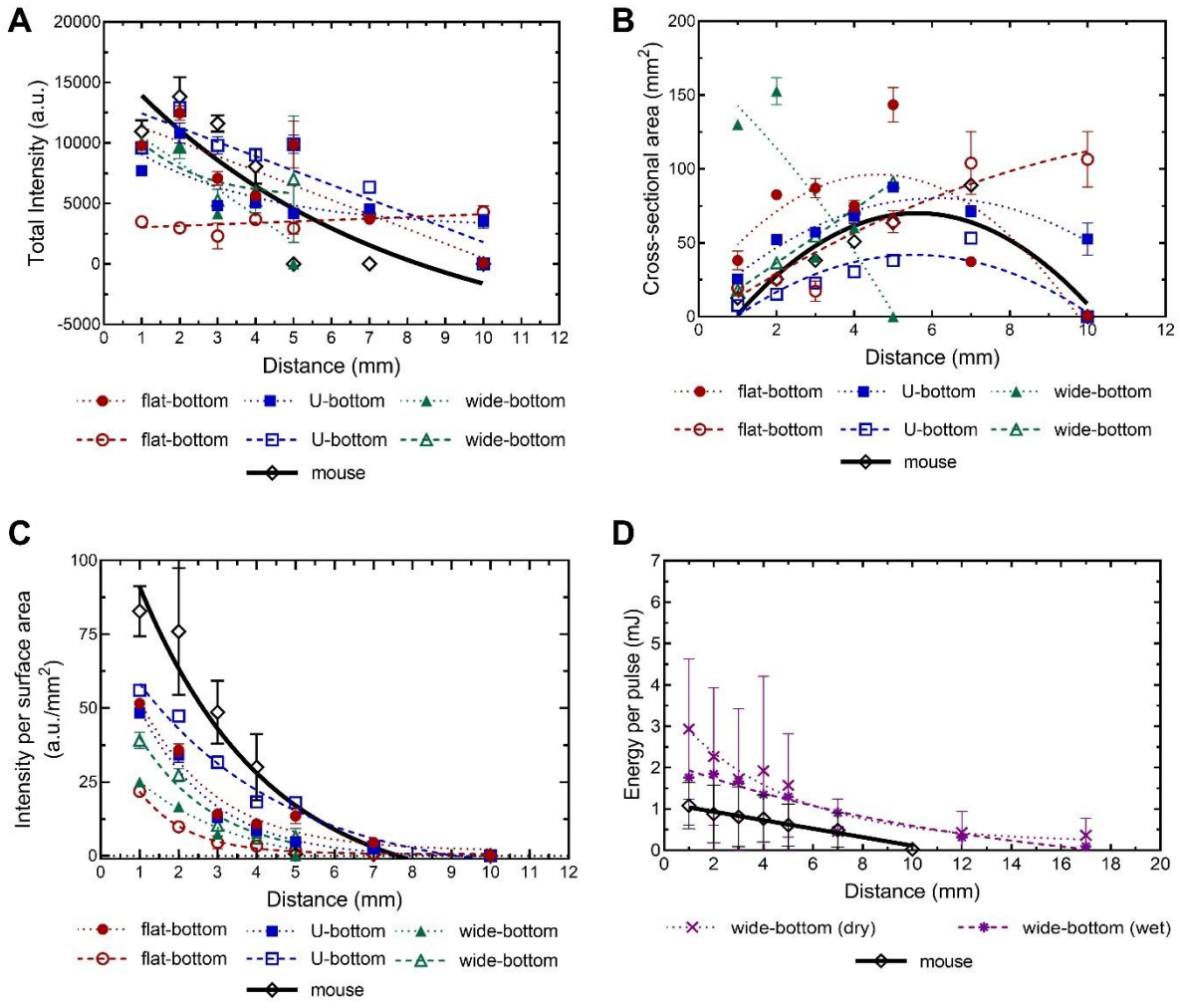

Figure 7. Comparison of DBD plasma discharge on plastic cell culture plates and mouse skin. The A) intensity, B) cross-sectional area, and C) intensity per surface area of the plasma discharge was calculated for DBD plasma generated on the dry (dashed lines) and wet (dotted lines) well plates, as well as the mouse skin (solid line). The voltage and current of a single DBD pulse were measured on the flat-bottom plate (both dry and wet) and the mouse skin, and D) the energy per pulse was calculated over a range of distances. A non-linear regression (centered second order polynomial for A, B, and D; one phase exponential decay for C) was used to fit all data. Data are represented as mean ± standard deviation (n = 3 – 13). Abbreviations: flat-bottom (96-well flat bottom plate), U-bottom (96-well U-bottom plate), wide-bottom (24-well flat bottom plate).

Comparison of optical emission spectra of DBD plasma discharge on plastic cell culture plates and mouse skin

In order to further investigate the DBD plasma discharge on cell culture plates and mouse skin, optical emission spectroscopy (OES) was performed. A 1 mm application distance was used for all measurements, as is commonly used in plasma medicine studies, and a range of plasma pulse frequencies were assessed. All investigated systems (i.e. dry wide-bottom plate, wet wide-bottom plate, and mouse skin) demonstrated the same sets of emission structures (Figure 8A) that correspond to the presence of ●NO radicals ($NO(A^2\Sigma^+\text{-}X^2\Pi)$), ●OH radicals ($OH(A^2\Sigma^+\text{-}X^2\Pi)$), electronically excited N_2 (see below), N_2^+ ions ($N_2^+(B^2\Sigma_u\text{-}X^2\Sigma_g)$ – first negative system (FNS)), and atomic ●O ($3^5P_{1,2,3}\text{-}3^5S_0$ at 777 nm). The electronically excited N_2 include the so-called second positive system (SPS) - $N_2(C^3\Pi_u\text{-}B^3\Pi_g)$ and the first positive system (FPS) - $N_2(B_3\Pi_g\text{-}A^3\Pi_g)$), and the presence of atomic ●O indicates the formation of O_3 and the involvement in the ●NO radical generation.

The reduced electric field (*E/n)* values were roughly the same (within the error bars) for the dry (369 ± 11 Td) and wet (360 ± 26 Td) wide-bottom well plates, and were slightly reduced for the mouse system (334 ± 7 Td) (Figure 8B). For all investigated system arrangements, T_{gas} was found to be 328 ± 10 K, as measured from a fitted spectrum of $N_2(C_3\Pi_u\text{-}B_3\Pi_g, \Delta v = 0)$ (Figure 8C). Interestingly, the vibrational temperature (T_{vib}) of the N_2 electronically excited levels was significantly higher on the mouse skin (3856 ± 268 K) compared to the cell culture plates (3198 ± 345 K), regardless of the applied plasma pulse frequency (Figure 8D). This could be due to O_3 accumulation in the enclosed, well plate system. N_2 electronically excited states can be directly quenched by O_3 molecules [56], or more probably, via a two steps mechanism which includes O_3 dissociation with the formation of ●O atoms, and consequent quenching of $N_2(C_3\Pi_u)$ by ●O [56] forming ●NO radicals [57].

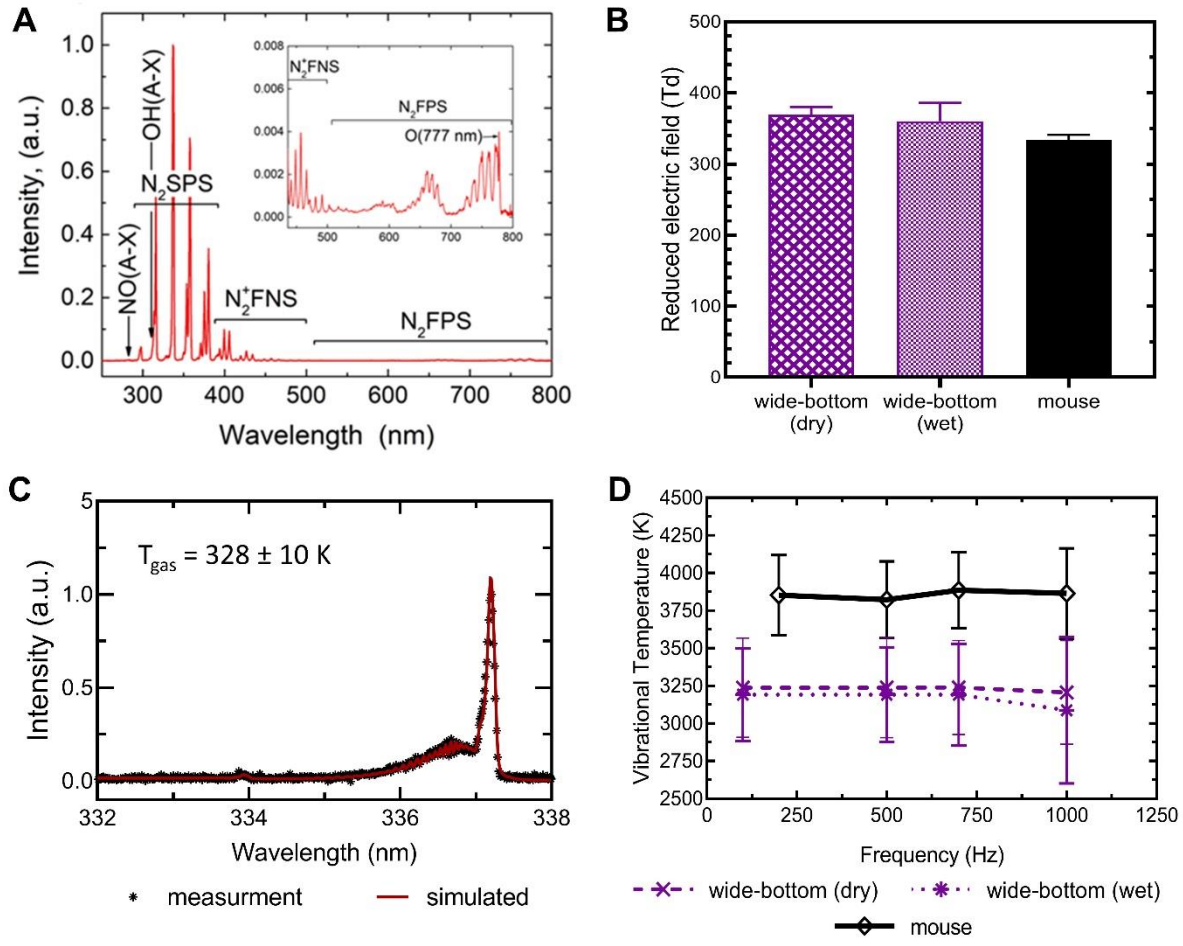

Figure 8. OES characterization of DBD plasma on cell culture well plates and mouse skin. A) Example of full spectrum of the DBD plasma at 1000 Hz pulse frequency; the spectra look similar for all investigated conditions. B) Reduced electric field values for dry well, wet well, and mouse skin. C) Best fit of the measured and simulated spectra of $N_2(C^3\Pi_u\text{-}B^3\Pi_g, \Delta v = 0)$ rotational structure for the 1000 Hz discharge generated above the mouse, to determine the gas temperature (T_{gas}); it was found to be the same for all investigated conditions. D) Vibrational temperature of the N_2 electronically excited levels, measured at different discharge frequencies.

While the DBD plasma pulse frequency did not affect the gas or vibrational temperature, we observed an increase in the emission intensity upon pulse frequency of all detected transitions (Figure 9A). This can be simply explained by an increase in the plasma pulse frequency, which leads to an increase in the number of generated plasma breakdown events. Based on the intensity ratios, we can obtain information on the density (but only in relative units) of ground states of ●OH, atomic ●O, and ●NO using the corona approximation described in the "Experimental methods" part. For DBD plasma treatment of both the cell culture plates and the mouse skin, the ●OH and atomic ●O density increased with increasing plasma pulse frequency (Figure 9B, C). In fact, this is in-line with our previous experiments, where we investigated which DBD plasma-generated species were most responsible for immunogenic

cancer cell death (ICD) [8, 9]. Using electron paramagnetic resonance (EPR) spectroscopy, we identified aqueous ●OH, ●O/O_3, and ●NO as the most critical plasma-generated species for inducing cancer ICD signals, which increased as plasma treatment intensity (pulse frequency) was increased [9]. In this work, we not only identify the presence of ●OH and ●O in the gas phase, but also observed their pulse frequency-dependent trends (Figure 9B, C). Interestingly, for all systems, the ●NO density decreased with increasing plasma pulse frequency. This could be prescribed to accumulation of O_3 in the systems that leads to an efficient ●NO oxidation to NO_2 via the reaction: $O_3 + NO \rightarrow NO_2 + O_2$ [58]. In the context of our previous work on DBD plasma-induced cancer ICD, these data suggest that ●NO may not be a major effector for this specific biological response. However, these data highlight the importance of determining which plasma-generated species are most critical for a specific biological response, as the optimal generation and delivery of different species may require different plasma treatment strategies.

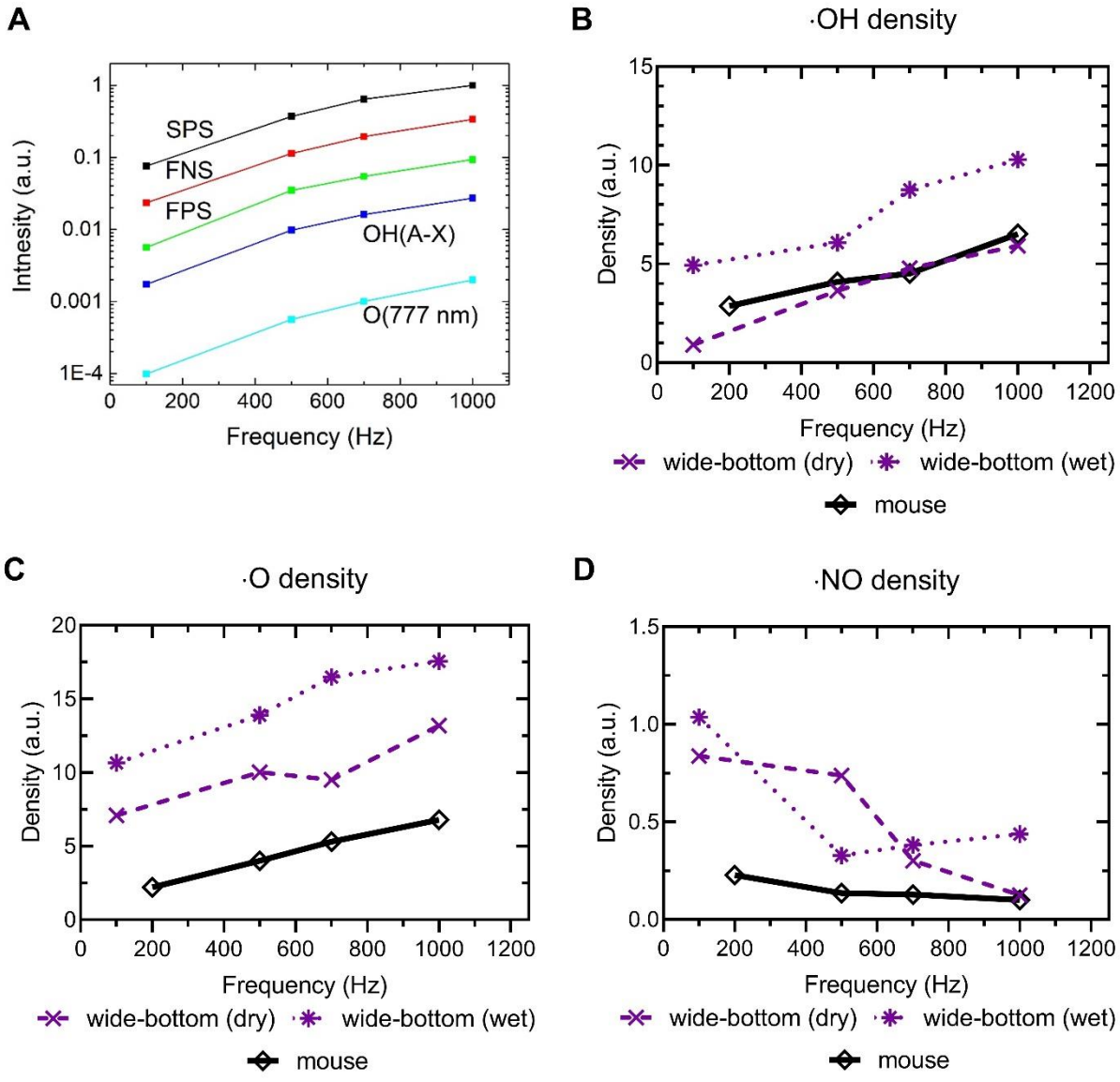

Figure 9. Quantification of radical species from optical emission intensities. A) Example of optical emission intensities: SPS – second positive system of $N_2(C^3\Pi_u\text{-}B^3\Pi_g)$; FNS – first negative system of $N_2^+(B^2\Sigma_u\text{-}X^2\Sigma_g)$; FPS – first positive system of $N_2(B_3\Pi_g\text{-}A^3\Pi_g)$; OH(A-X) – rotational structure of $OH(A^2\Sigma^+\text{-}X^2\Pi)$ transition; O(777 nm) – atomic oxygen triplet $(3^5P_{1,2,3}\text{-}3^5S_0)$. B) ●OH radical, atomic ●O, and ●NO radical specie densities (in arbitrary units) were derived from the intensity ratios, for the various DBD plasma treatment systems, as a function of pulse frequency.

Conclusion

Industrial applications of DBDs have expanded beyond their original application to include surface modifications, pollution control, and most recently medicine. In life sciences applications, DBD systems use the biological target as the secondary electrode for direct plasma generation and treatment, and therefore, are sensitive to the surface properties of the target. Since most biological studies progress from *in vitro* experiments with cells in plasma cell culture plates to *in vivo* experiments on animal

research models such as mice, the DBD plasma interaction with the biological target could greatly differ. Therefore, in this study, we investigated the DBD plasma behavior in both *in vitro* (cell culture well plates) and *in vivo* (mouse skin) settings. DBD plasma application on both cell culture plates as well as mouse skin generated the same reactive species, namely ●OH, atomic ●O, and ●NO, as measured with OES. Well plate geometry and surface wetness (i.e., wet vs dry well plates) both affect DBD plasma discharge behavior, especially in the uniformity of the plasma across the bottom of the well. Here, the plasma generated on wet wide-bottom well plates was most visibly similar to that generated on mouse skin. Interestingly, in all *in vitro* and *in vivo* experimental settings, we observed that the DBD plasma intensity per surface area of treatment demonstrated an exponential one-phase decay with increasing application distance. Thus, monitoring DBD plasma intensity per surface area could be applied to account for the different treatment systems used in plasma medicine studies. This behavior was similar to the change in energy per pulse of the DBD plasma across a range of application distances. The energy per pulse is used to quantify the delivered plasma treatment energy, which we hypothesized is a major effector in dictating biological response [27].

Taken together, this study highlights that regardless of the system, quantification of DBD plasma intensity per surface area may be a valuable method for *in situ* monitoring during biological treatment, though further studies and validation are still required. The simplicity of this method could facilitate active plasma treatment control and monitoring 'plasma treatment dose', especially during complex cases of biomedical treatments both in the lab and potentially in the clinic.

Acknowledgements

This work was partially funded by the Research Foundation—Flanders (FWO) and supported by the following Grants: 12S9221N (A. L.), G044420N (A. L. and A. B.), and G033020N (A.B.). We would also like to thank several patrons, as part of this research was funded by donations from different donors, including Dedert Schilde vzw, Mr Willy Floren, and the Vereycken family. We would also like to acknowledge the support from the European Cooperation in Science & Technology (COST) Action on "Therapeutical applications of Cold Plasmas" (CA20114; PlasTHER)

Declarations

Ethical Approval

All animal experiments were approved by the University of Antwerp Animal Research Ethical Committee (ECD-dossier 2017-53).

Competing interests

Authors declare no competing interest.

Authors' contributions

Conceptualization: [A.L.]; Methodology: [A.L. and M.G.]; Formal analysis and investigation: [M.G. and A.L.]; Writing - original preparation [A.L. and M.G.]; Writing - review and editing [A.L, M.G., A.N., E.S., and A.B.]; Funding acquisition: [A.L. and A.B.]; Resources: [A.N., E.S., and A.B.]; Supervision [A.N., E.S., and A.B.]

Funding

This work was partially funded by the Research Foundation—Flanders (FWO) and supported by the following Grants: 12S9221N (A. L.), G044420N (A. L. and A. B.), and G033020N (A.B.).

Availability of data and materials

The datasets used in the current study are available from the corresponding author on reasonable request

APPENDIX I – Constants used for excited species calculations

Table 1X. Einstein transition coefficients and excitation energies

Transition	Einstein coefficient, s^{-1}	Excitation energy, eV	Ref.
NO($A^2\Sigma^+$–$X^2\Pi$)	9.8×10^5	5.48	[59, 60]
OH($A^2\Sigma^+$–$^2\Pi$)	8.6×10^5	4.01	[60, 61]
O (3^5P–3^5S)	28.6×10^6	10.74	[60, 62]

Table 2X. Rate coefficients (10^{-10} cm^3 s^{-1}) for NO($A^2\Sigma^+$), OH($A^2\Sigma^+$), and O(3S) quenching by N_2, O_2, and H_2O

Quencher	NO($A^2\Sigma^+$)	OH($A^2\Sigma^+$)	O(3^5P)	Ref.
N_2	0.0037	0.378	5.9	[63-65]
O_2	1.51	1.35	9.4	[63, 64, 66]
H_2O	7.7	6.56	49	[64, 67, 68]

Appendix II – DBD plasma on dry cell culture plates with different pulse frequencies and application distances

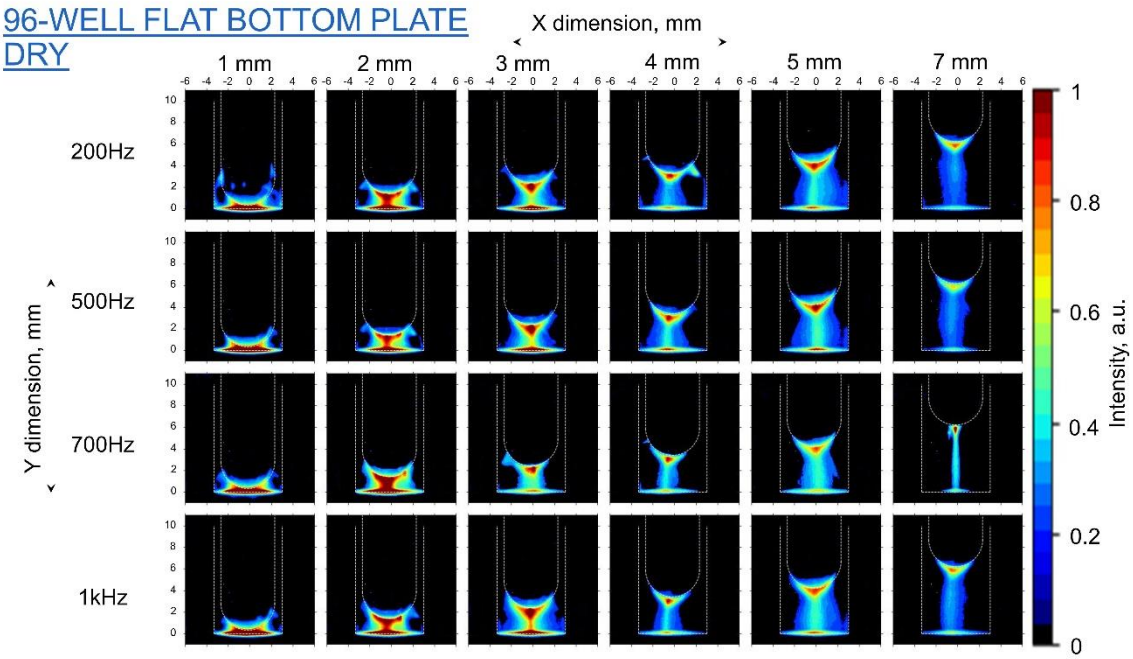

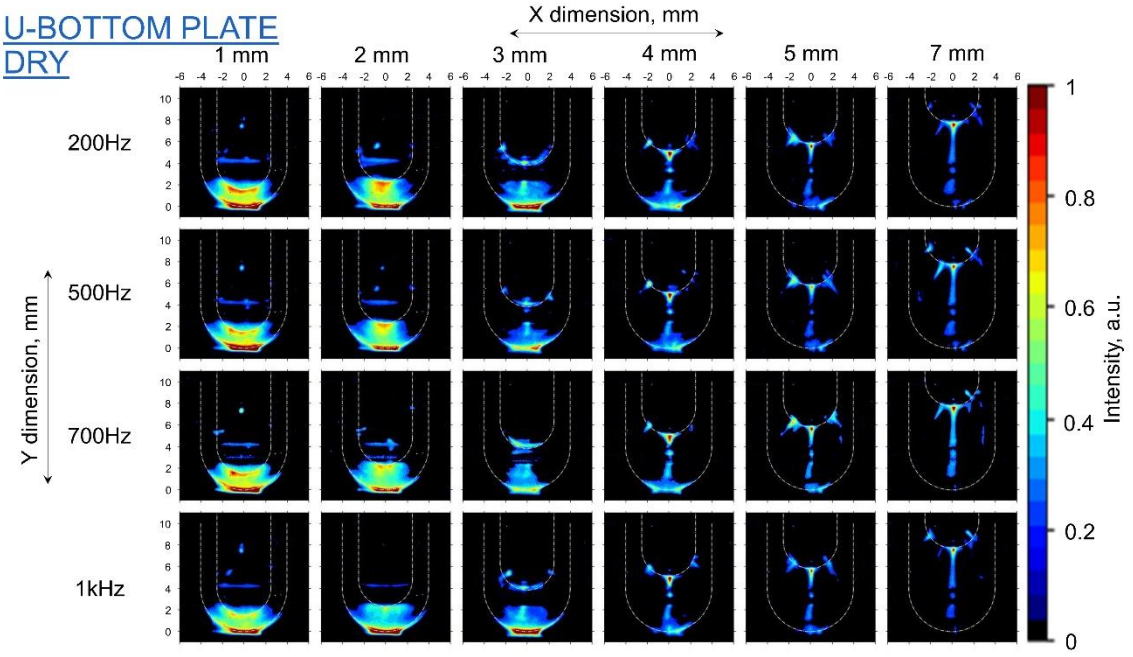

WIDE-BOTTOM PLATE
DRY

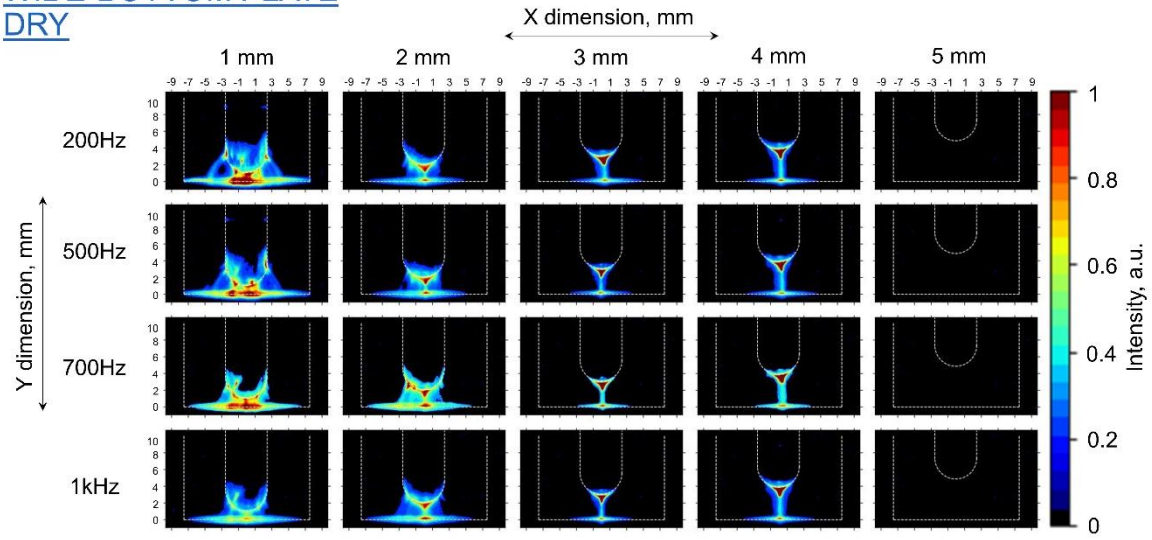

APPENDIX III – DBD plasma on wet cell culture plates with different pulse frequencies and application distances

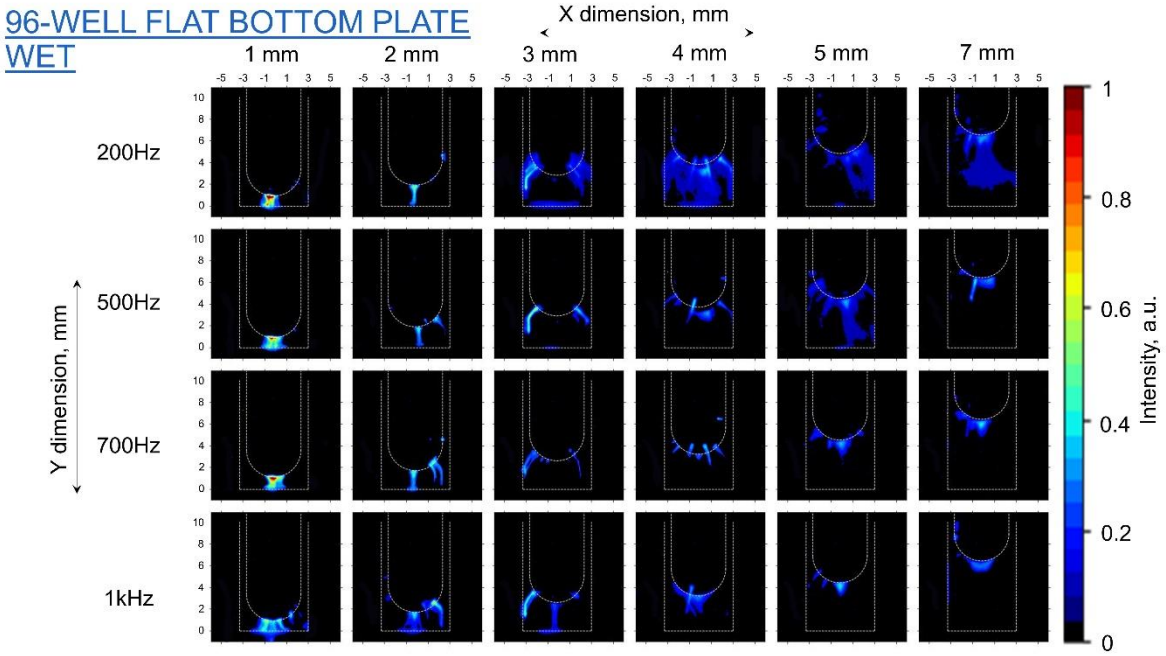

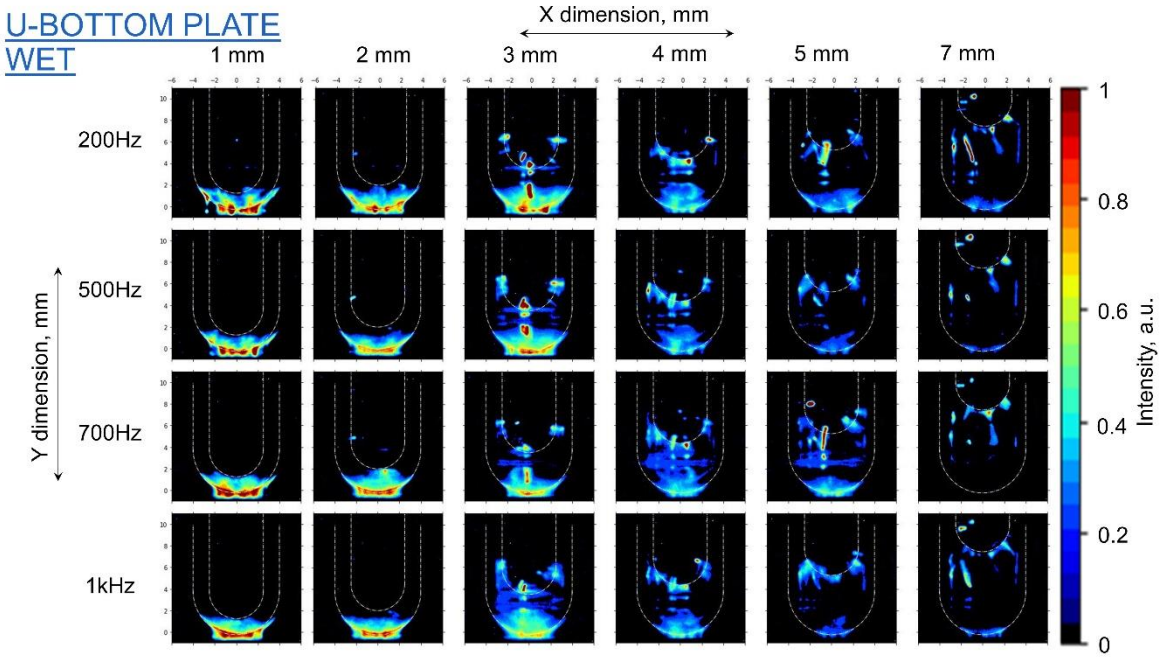

WIDE-BOTTOM PLATE
WET

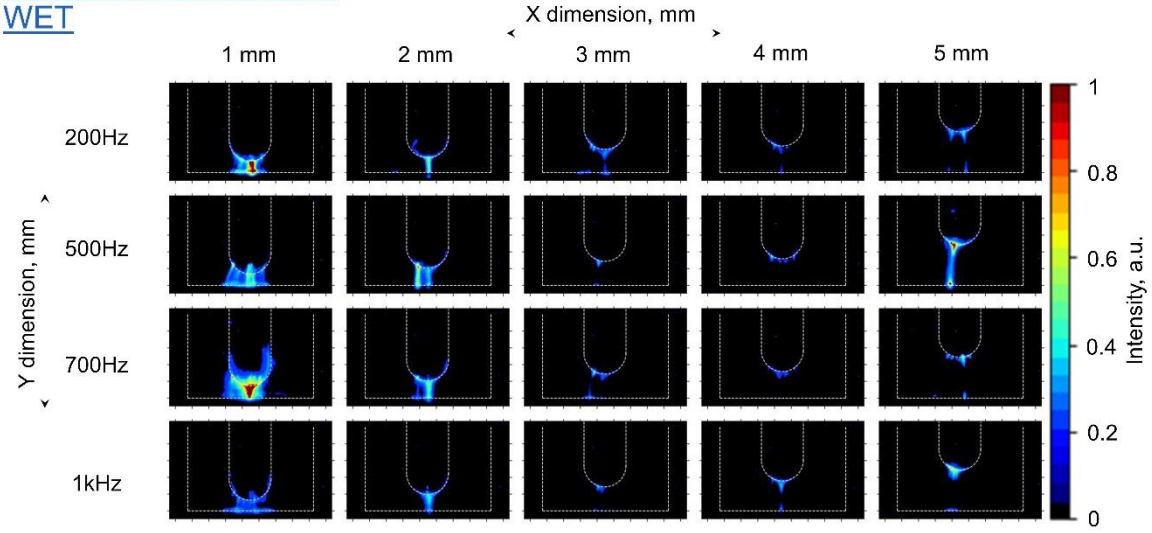

APPENDIX IV – DBD plasma on mouse skin with different pulse frequencies and application distances

MOUSE: 700 HZ

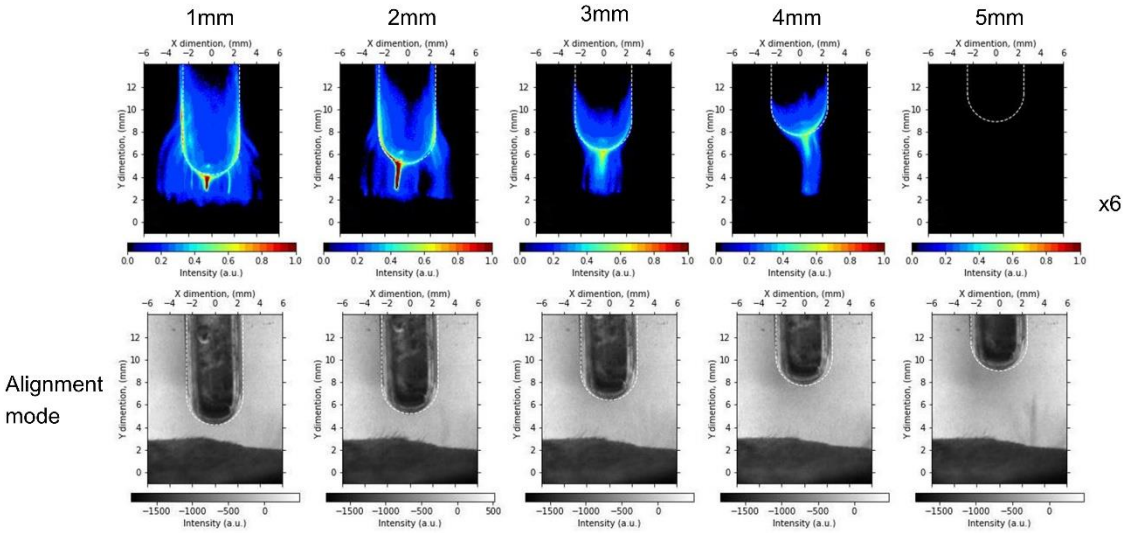

MOUSE: 1000 HZ

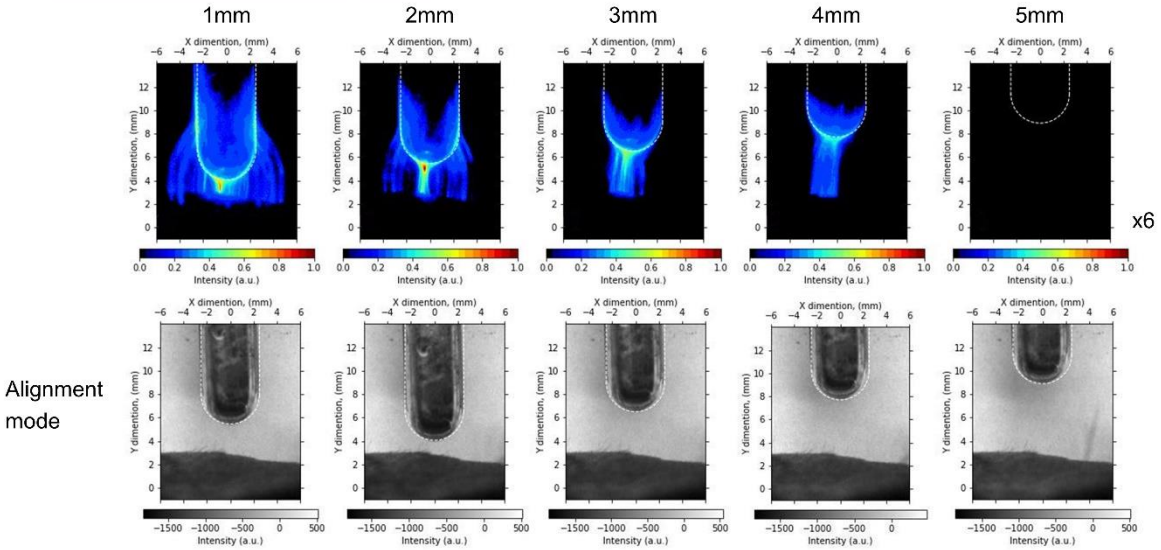

APPENDIX V– Quantification of DBD plasma surface area and volume on *in vitro* well plates, both dry (dashed lines) and wet (dotted lines), and *in vivo* mouse skin at different application distances

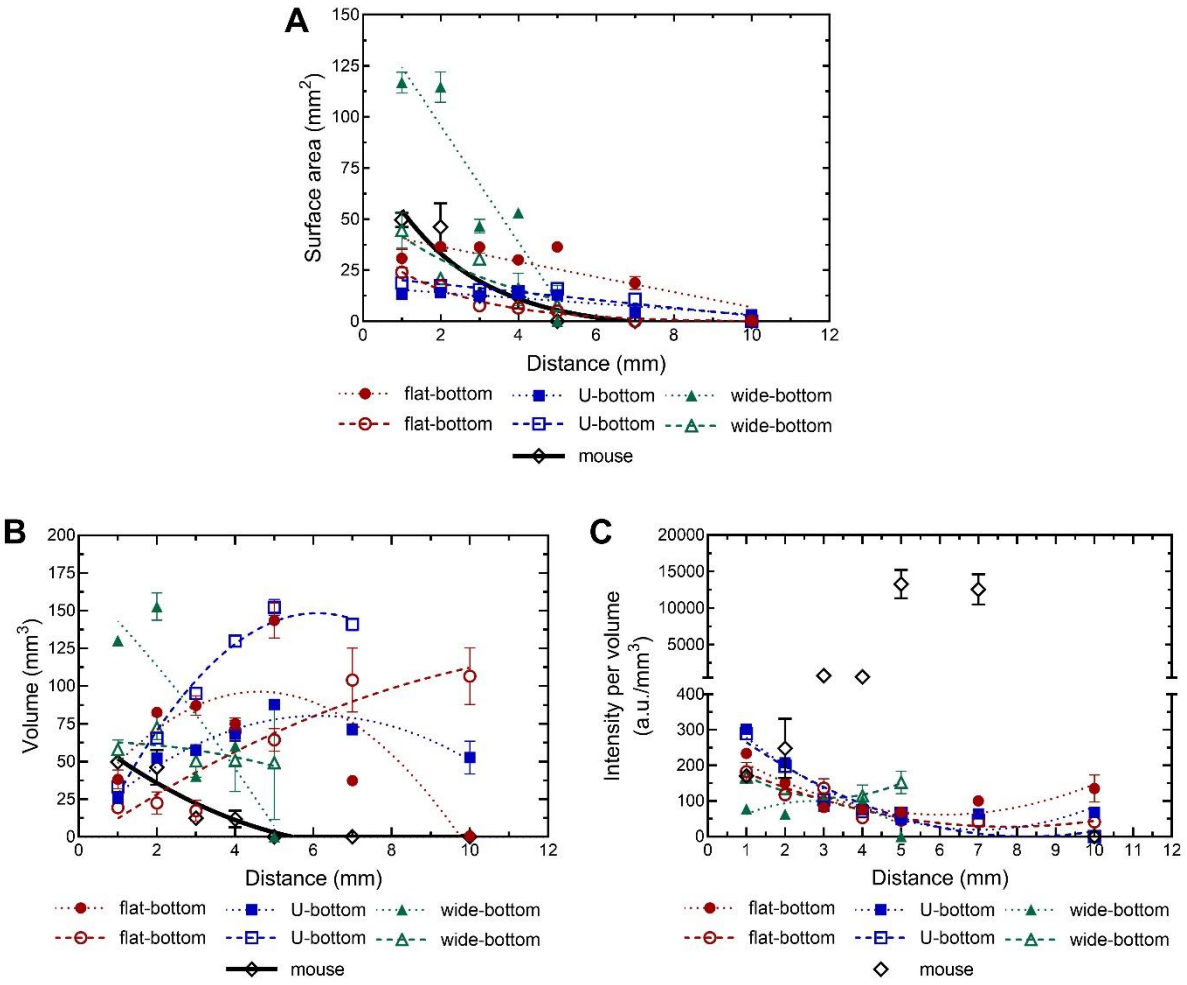

References

1. Fridman, A., A. Chirokov, and A. Gutsol, *Non-thermal atmospheric pressure discharges.* Journal of Physics D: Applied Physics, 2005. **38**(2): p. R1.
2. Borcia, G., C. Anderson, and N. Brown, *Dielectric barrier discharge for surface treatment: application to selected polymers in film and fibre form.* Plasma Sources Science and Technology, 2003. **12**(3): p. 335.
3. Carman, R., D. Kane, and B. Ward, *Enhanced performance of an EUV light source (λ= 84 nm) using short-pulse excitation of a windowless dielectric barrier discharge in neon.* Journal of Physics D: Applied Physics, 2009. **43**(2): p. 025205.
4. Li, S., et al., *The application of dielectric barrier discharge non-thermal plasma in VOCs abatement: A review.* Chemical Engineering Journal, 2020. **388**: p. 124275.
5. Kogelschatz, U., *Dielectric-barrier discharges: their history, discharge physics, and industrial applications.* Plasma Chemistry and Plasma Processing, 2003. **23**(1): p. 1-46.
6. Privat-Maldonado, A., et al., *Ros from physical plasmas: Redox chemistry for biomedical therapy.* Oxidative medicine cellular longevity, 2019. **2019**.
7. Lin, A., et al., *The effect of local non-thermal plasma therapy on the cancer-immunity cycle in a melanoma mouse model.* Bioengineering & Translational Medicine, 2022: p. e10314.
8. Lin, A., et al., *Nanosecond-Pulsed DBD Plasma-Generated Reactive Oxygen Species Trigger Immunogenic Cell Death in A549 Lung Carcinoma Cells through Intracellular Oxidative Stress.* International Journal of Molecular Sciences, 2017. **18**(5): p. 966.
9. Lin, A., et al., *Non-Thermal plasma as a unique delivery system of short-lived reactive oxygen and nitrogen species for immunogenic cell death in melanoma cells.* Advanced Science, 2019. **6**(6): p. 1802062.
10. Bekeschus, S., et al., *Oxygen atoms are critical in rendering THP-1 leukaemia cells susceptible to cold physical plasma-induced apoptosis.* Scientific reports, 2017. **7**(1): p. 1-12.
11. Chernets, N., et al., *Reaction Chemistry Generated by Nanosecond Pulsed Dielectric Barrier Discharge Treatment is Responsible for the Tumor Eradication in the B16 Melanoma Mouse Model.* Plasma Processes and Polymers, 2015.
12. Ikehara, Y., et al., *Formation of membrane-like structures in clotted blood by mild plasma treatment during hemostasis.* Journal of Photopolymer Science and Technology, 2013. **26**(4): p. 555-557.
13. Kim, J., et al., *Coagulation, deformability, and aggregation of RBCs and platelets following exposure to dielectric barrier discharge plasma with the use of different feeding gases.* Journal of Physics D-Applied Physics, 2019. **52**(15).
14. Ding, C.B., et al., *Immediate intervention effect of dielectric barrier discharge on acute inflammation in rabbit's ear wound.* Aip Advances, 2020. **10**(2).
15. Brehmer, F., et al., *Alleviation of chronic venous leg ulcers with a hand-held dielectric barrier discharge plasma generator (PlasmaDerm((R)) VU-2010): results of a monocentric, two-armed, open, prospective, randomized and controlled trial (NCT01415622).* J Eur Acad Dermatol Venereol, 2015. **29**(1): p. 148-55.
16. Heuer, K., et al., *The topical use of non-thermal dielectric barrier discharge (DBD): nitric oxide related effects on human skin.* Nitric Oxide, 2015. **44**: p. 52-60.
17. Katiyar, K.S., et al., *Non-thermal plasma accelerates astrocyte regrowth and neurite regeneration following physical trauma in vitro.* Applied Sciences, 2019. **9**(18): p. 3747.
18. Mitra, S., et al., *Utility of Reactive Species Generation in Plasma Medicine for Neuronal Development.* Biomedicines, 2020. **8**(9): p. 348.
19. Jang, J.Y., et al., *Cold atmospheric plasma (CAP), a novel physicochemical source, induces neural differentiation through cross-talk between the specific RONS cascade and Trk/Ras/ERK signaling pathway.* Biomaterials, 2018. **156**: p. 258-273.
20. Sahun, M., et al., *Inactivation of SARS-CoV-2 and Other Enveloped and Non-Enveloped Viruses with Non-Thermal Plasma for Hospital Disinfection.* ACS Sustain Chem Eng, 2023. **11**(13): p. 5206-5215.

21. Ma, Y., et al., *Chemical mechanisms of bacterial inactivation using dielectric barrier discharge plasma in atmospheric air.* Ieee Transactions on Plasma Science, 2008. **36**(4): p. 1615-1620.
22. Olatunde, O.O., S. Benjakul, and K. Vongkamjan, *Dielectric barrier discharge cold atmospheric plasma: Bacterial inactivation mechanism.* Journal of Food Safety, 2019. **39**(6).
23. Lin, A., et al., *Acquired non-thermal plasma resistance mediates a shift towards aerobic glycolysis and ferroptotic cell death in melanoma.* Drug Resist Updat, 2023. **67**: p. 100914.
24. Lin, A., et al., *Oxidation of Innate Immune Checkpoint CD47 on Cancer Cells with Non-Thermal Plasma.* Cancers, 2021. **13**(3): p. 579.
25. Panngom, K., et al., *Preferential killing of human lung cancer cell lines with mitochondrial dysfunction by nonthermal dielectric barrier discharge plasma.* Cell Death Dis, 2013. **4**(5): p. e642.
26. Lu, X., et al., *Grand challenges in low temperature plasmas.* Frontiers in Physics, 2022: p. 1036.
27. Lin, A., et al., *Toward defining plasma treatment dose: The role of plasma treatment energy of pulsed-dielectric barrier discharge in dictating in vitro biological responses.* Plasma Processes and Polymers, 2022. **19**(3).
28. Simoncelli, E., et al., *Experimental investigation on the influence of target physical properties on an impinging plasma jet.* Plasma, 2019. **2**(3): p. 369-379.
29. Lin, A., et al., *Non-Equilibrium Dielectric Barrier Discharge Treatment of Mesenchymal Stem Cells: Charges and Reactive Oxygen Species Play the Major Role in Cell Death.* Plasma Processes and Polymers, 2015.
30. Gherardi, M., et al., *Atmospheric non-equilibrium plasma promotes cell death and cell-cycle arrest in a lymphoma cell line.* Plasma Processes and Polymers, 2015. **12**(12): p. 1354-1363.
31. Babaeva, N.Y. and M.J. Kushner, *Reactive fluxes delivered by dielectric barrier discharge filaments to slightly wounded skin.* Journal of Physics D: Applied Physics, 2012. **46**(2): p. 025401.
32. Van der Paal, J., et al., *Interaction of O and OH radicals with a simple model system for lipids in the skin barrier: a reactive molecular dynamics investigation for plasma medicine.* Journal of Physics D: Applied Physics, 2013. **46**(39): p. 395201.
33. Stancampiano, A., et al., *Mimicking of human body electrical characteristic for easier translation of plasma biomedical studies to clinical applications.* IEEE Transactions on Radiation and Plasma Medical Sciences, 2019. **4**(3): p. 335-342.
34. Lin, A., et al., *Critical Evaluation of the Interaction of Reactive Oxygen and Nitrogen Species with Blood to Inform the Clinical Translation of Nonthermal Plasma Therapy.* 2020. **2020**.
35. Verswyvel, H., et al., *Phototoxicity and cell passage affect intracellular reactive oxygen species levels and sensitivity towards non-thermal plasma treatment in fluorescently-labeled cancer cells.* Journal of Physics D: Applied Physics, 2023. **56**(29): p. 294001.
36. Lin, A., et al., *Critical Evaluation of the Interaction of Reactive Oxygen and Nitrogen Species with Blood to Inform the Clinical Translation of Nonthermal Plasma Therapy.* Oxidative medicine cellular longevity, 2020. **2020**.
37. Bruggeman, P., et al., *Gas temperature determination from rotational lines in non-equilibrium plasmas: a review.* Plasma Sources Science and Technology, 2014. **23**(2): p. 023001.
38. Sremački, I., et al., *An atmospheric pressure non-self-sustained glow discharge in between metal/metal and metal/liquid electrodes.* Plasma Processes and Polymers, 2020. **17**(6): p. 1900191.
39. Voráč, J., et al., *Batch processing of overlapping molecular spectra as a tool for spatio-temporal diagnostics of power modulated microwave plasma jet.* Plasma Sources Science and Technology, 2017. **26**(2): p. 025010.
40. Voráč, J., et al., *State-by-state emission spectra fitting for non-equilibrium plasmas: OH spectra of surface barrier discharge at argon/water interface.* Journal of Physics D: Applied Physics, 2017. **50**(29): p. 294002.
41. Olszewski, P., et al., *Measurement and control of the streamer head electric field in an atmospheric-pressure dielectric barrier plasma jet.* Plasma Sources Science and Technology, 2014. **23**(1): p. 015010.

42. Bílek, P., et al., *Electric field determination in air plasmas from intensity ratio of nitrogen spectral bands: II. Reduction of the uncertainty and state-of-the-art model.* Plasma Sources Science and Technology, 2018. **27**(8): p. 085012.
43. Vervloessem, E., et al., *NH3 and HNO x Formation and Loss in Nitrogen Fixation from Air with Water Vapor by Nonequilibrium Plasma.* ACS Sustainable Chemistry & Engineering, 2023. **11**(10): p. 4289-4298.
44. Ricciardi, E.F., et al., *Effects of plasma treatments applied to fresh ricotta cheese.* Innovative Food Science & Emerging Technologies, 2022. **76**: p. 102935.
45. Miller, V., et al., *Plasma Stimulation of Migration of Macrophages.* Plasma Processes and Polymers, 2014. **11**(12): p. 1193-1197.
46. Olatunde, O.O., S. Benjakul, and K. Vongkamjan, *Dielectric barrier discharge cold atmospheric plasma: Bacterial inactivation mechanism.* Journal of Food Safety, 2019. **39**(6): p. e12705.
47. Kimlin, L.C., G. Casagrande, and V.M. Virador, *In vitro three-dimensional (3D) models in cancer research: an update.* Molecular carcinogenesis, 2013. **52**(3): p. 167-182.
48. Deshayes, N., et al., *3D In vitro model of the re-epithelialization phase in the wound-healing process.* Experimental Dermatology, 2018. **27**(5): p. 460-462.
49. Privat-Maldonado, A., et al., *Reduction of human glioblastoma spheroids using cold atmospheric plasma: The combined effect of short-and long-lived reactive species.* Cancers, 2018. **10**(11): p. 394.
50. Hasse, S., et al., *Plasma treatment limits human melanoma spheroid growth and metastasis independent of the ambient gas composition.* Cancers, 2020. **12**(9): p. 2570.
51. Judée, F., et al., *Short and long time effects of low temperature Plasma Activated Media on 3D multicellular tumor spheroids.* Scientific reports, 2016. **6**(1): p. 21421.
52. Gokcelli, U., et al., *Prevention of Peritoneal Adhesions by Non-Thermal Dielectric Barrier Discharge Plasma Treatment on Mouse Model: A Proof of Concept Study.* J Invest Surg, 2020. **33**(7): p. 605-614.
53. Chernets, N., et al., *Nonthermal atmospheric pressure plasma enhances mouse limb bud survival, growth, and elongation.* Tissue Engineering Part A, 2014. **21**(1-2): p. 300-309.
54. Heuer, K., et al., *The topical use of non-thermal dielectric barrier discharge (DBD): nitric oxide related effects on human skin.* Nitric Oxide, 2015. **44**: p. 52-60.
55. Brehmer, F., et al., *Alleviation of chronic venous leg ulcers with a hand-held dielectric barrier discharge plasma generator (PlasmaDerm® VU-2010): results of a monocentric, two-armed, open, prospective, randomized and controlled trial (NCT 01415622).* Journal of the European Academy of Dermatology and Venereology, 2015. **29**(1): p. 148-155.
56. Adamovich, I., et al., *Plasma assisted ignition and high-speed flow control: non-thermal and thermal effects.* Plasma Sources Science and Technology, 2009. **18**(3): p. 034018.
57. Popov, N. and S. Starikovskaia, *Relaxation of electronic excitation in nitrogen/oxygen and fuel/air mixtures: fast gas heating in plasma-assisted ignition and flame stabilization.* Progress in Energy and Combustion Science, 2022. **91**: p. 100928.
58. Abdelaziz, A.A. and H.-H. Kim, *Temperature-dependent behavior of nitrogen fixation in nanopulsed dielectric barrier discharge operated at different humidity levels and oxygen contents.* Journal of Physics D: Applied Physics, 2020. **53**(11): p. 114001.
59. Luque, J. and D.R. Crosley, *Transition probabilities and electronic transition moments of the A 2 Σ+–X 2 Π and D 2 Σ+–X 2 Π systems of nitric oxide.* The Journal of chemical physics, 1999. **111**(16): p. 7405-7415.
60. Ochkin, V.N., *Spectroscopy of low temperature plasma*. 2009: John Wiley & Sons.
61. Becker, K. and D. Haaks, *Measurement of the natural lifetimes and quenching rate constants of OH (2Σ+, v= 0, 1) and OD (2Σ+, v= 0, 1) radicals.* Zeitschrift Für Naturforschung A, 1973. **28**(2): p. 249-256.
62. Settersten, T.B., B.D. Patterson, and J.A. Gray, *Temperature-and species-dependent quenching of NO AΣ+ 2 (v'=) probed by two-photon laser-induced fluorescence using a picosecond laser.* The Journal of chemical physics, 2006. **124**(23).
63. Nee, J., et al., *The electronic quenching rates of NO (A2Σ+, v'= 0–2).* Chemical physics, 2004. **300**(1-3): p. 85-92.

64. Martini, L.M., et al., *Rate constants of quenching and vibrational relaxation in the OH (), manifold with various colliders.* Journal of Physics D: Applied Physics, 2017. **50**(11): p. 114003.
65. Niemi, K., V. Schulz-Von Der Gathen, and H. Döbele, *Absolute calibration of atomic density measurements by laser-induced fluorescence spectroscopy with two-photon excitation.* Journal of Physics D: Applied Physics, 2001. **34**(15): p. 2330.
66. Niemi, K., V. Schulz-Von Der Gathen, and H. Döbele, *Absolute atomic oxygen density measurements by two-photon absorption laser-induced fluorescence spectroscopy in an RF-excited atmospheric pressure plasma jet.* Plasma Sources Science and Technology, 2005. **14**(2): p. 375.
67. McDermid, I.S. and J.B. Laudenslager, *Radiative lifetimes and electronic quenching rate constants for single-photon-excited rotational levels of NO (A2Σ+, v'= 0).* Journal of Quantitative Spectroscopy and Radiative Transfer, 1982. **27**(5): p. 483-492.
68. Bittner, J., et al., *Quenching of two-photon-excited H (3s, 3d) and O (3p 3P2, 1, 0) atoms by rare gases and small molecules.* Chemical Physics Letters, 1988. **143**(6): p. 571-576.